NEUROSCIENCE

Brain injury environment critically influences the connectivity of transplanted neurons

Sofia Grade[1,2]*†, Judith Thomas[1,2,3], Yvette Zarb[1,2], Manja Thorwirth[1,2], Karl-Klaus Conzelmann[4], Stefanie M. Hauck[5]*, Magdalena Götz[1,2,6]*

Cell transplantation is a promising approach for the reconstruction of neuronal circuits after brain damage. Transplanted neurons integrate with remarkable specificity into circuitries of the mouse cerebral cortex affected by neuronal ablation. However, it remains unclear how neurons perform in a local environment undergoing reactive gliosis, inflammation, macrophage infiltration, and scar formation, as in traumatic brain injury (TBI). To elucidate this, we transplanted cells from the embryonic mouse cerebral cortex into TBI-injured, inflamed-only, or intact cortex of adult mice. Brain-wide quantitative monosynaptic rabies virus (RABV) tracing unraveled graft inputs from correct regions across the brain in all conditions, with pronounced quantitative differences: scarce in intact and inflamed brain versus exuberant after TBI. In the latter, the initial overshoot is followed by pruning, with only a few input neurons persisting at 3 months. Proteomic profiling identifies candidate molecules for regulation of the synaptic yield, a pivotal parameter to tailor for functional restoration of neuronal circuits.

INTRODUCTION

The adult mammalian brain poorly regenerates in the aftermath of an injury, and thus, strategies of neuronal transplantation have been pursued to rebuild circuits and restore behavioral function (*1*–*4*). Quantitative connectomics has enabled a fine comparison of the connections developed by transplants with those of their endogenous counterparts (*5*–*7*). Previous analysis in the mouse cortex has shown that new neurons mature and connect with the host brain in a remarkably correct manner, with high specificity both in their synaptic integration and in their response to external stimuli (*5*). The injury, in this case, consisted of the selective ablation of a cohort of neurons in the cortex by inducing apoptosis in the targeted neurons and implied little inflammatory reaction, no glial scar, or brain-blood barrier breakdown (*8*).

While these findings are encouraging, it remains open whether accurate graft connectivity is achieved in more clinically relevant injuries like a traumatic brain injury (TBI), which provide a distinctive cellular and molecular milieu. While several transplantation studies described a bystander effect via neuroprotection and immunomodulation in TBI (*9*–*12*), still little is known about neuronal replacement and brain-wide connectivity in this injury. This has been probed only using grafts with low amounts of mature neurons and lacking full and quantitative connectivity analysis (*13*). Here, we analyzed graft connectivity in a mouse model of penetrating TBI. TBI results in severe reactive gliosis and scar formation, with infiltration of phagocytic macrophages and accumulation of high content of inflammatory molecules (*14*–*16*). Molecular and cellular components of an injured brain parenchyma have been implicated in synapse pruning (*17*, *18*). One may hence predict deficits in the initial synaptic integration, as synapse formation may concur with uncontrollable pruning. Microglial cells, in particular, are critical for brain wiring and synapse pruning (*19*) and are the first responders to brain injury, swiftly adopting an activated phenotype and initiating neuroinflammation (*20*, *21*). To examine their contribution, we used a systemic injection of lipopolysaccharide (LPS), a well-documented inflammatory stimulus, as an additional condition complementing the TBI. LPS activates Toll-like receptor 4 (TLR4), which is specifically expressed by microglial cells in the rodent brain (*22*). To achieve the least damaged environment, we also transplanted into the intact cerebral cortex, only inflicted by the thin transplantation needle, as a third paradigm.

We also set out to study the maintenance of the initial connectivity. A phase of active synapse remodeling with a net gain was observed by live imaging in the neurites of transplanted neurons during the first month (*5*). This synapse turnover then gradually reached the basal turnover rate observed in the cortex of adult mice (*23*) at about 2 to 3 months after transplantation. However, the balance may be tilted toward an excessive elimination of new synapses in an environment characterized by a reactive and inflammatory state with large amount of pruning cells. The stability of the initial connectivity in TBI conditions remains unknown. Long-term connectivity is crucial for the successful outcome of a neuronal replacement therapy and needs to be ensured before clinical trials. Here, we investigated the role of the host microenvironment in the initial and long-term connectivity of neuronal transplants by using rabies virus (RABV)–mediated tracing and brain-wide quantitative connectomics, and leveraged proteomics to identify candidate molecules involved in the connectivity differences.

RESULTS

Transplanted neurons develop complex morphologies and synaptic protrusions in cortical stab injury

To produce a brain injury in the cerebral cortex of the adult mouse brain, we inflicted a stab injury or so-called stab wound (SW) within

[1]Physiological Genomics, Biomedical Center, Ludwig-Maximilians University Munich, 82152 Planegg-Martinsried, Germany. [2]Institute of Stem Cell Research, Helmholtz Center Munich, German Center for Environmental Health, 82152 Planegg-Martinsried, Germany. [3]Graduate School of Systemic Neuroscience, Ludwig-Maximilians University Munich, 82152 Planegg-Martinsried, Germany. [4]Max von Pettenkofer Institute Virology, Medical Faculty and Gene Center, Ludwig-Maximilians University Munich, 81377 Munich, Germany. [5]Research Unit Protein Science and Metabolomics and Proteomics Core, Helmholtz Center Munich, German Center for Environmental Health, 85764 Neuherberg, Germany. [6]SYNERGY, Excellence Cluster of Systems Neurology, Biomedical Center, Ludwig-Maximilians University Munich, 82152 Planegg-Martinsried, Germany.
*Corresponding author. Email: sofia.grade@imba.oeaw.ac.at (S.G.); hauck@helmholtz-muenchen.de (S.M.H.); magdalena.goetz@helmholtz-muenchen.de (M.G.)
†Present address: Institute of Molecular Biotechnology of the Austrian Academy of Sciences (IMBA), 1030 Vienna, Austria.

the primary visual cortex. The choice of the injury model rests on its high reproducibility and extensive knowledge about the temporal dynamics of wound healing, reactive gliosis, scar formation, as well as transcriptome and proteome (*15*, *16*, *24*–*26*). Donor cells from mouse embryonic cortex expressing green fluorescent protein (GFP) or red fluorescent protein (RFP) were transplanted into the center of the incision a week later and analyzed 5 days and 5 weeks post-transplantation (dpt/wpt; Fig. 1, A and B). Early, at 5 dpt, transplanted cells expressed the immature neuronal marker doublecortin (Dcx; Fig. 1C). By 5 wpt, the graft remained confined to the site of transplantation and injury, with no or little cell dispersion, and cells had developed complex arborizations of their neurites (Fig. 1, D to F). Cux1 immunolabeling demonstrated that most of the transplanted neurons displayed cortical upper layer identity (Fig. 1E and fig. S4B; with 70.27% of the transplanted cells expressing Cux1). These observations are in line with those in the neuronal ablation model with low inflammation (*5*). Note that Cux1 is also expressed in reelin$^+$ interneurons at early postnatal stages (*27*). Nevertheless, both the morphology observed here [also by live imaging in vivo in (*5*)] together with Cux1 and additionally Satb2 staining suggest that most transplanted neurons are pyramidal neurons, and at least some of callosal projection neuron identity (Satb2$^+$; fig. S4D). Inspection at high magnification shows that a complex network of axons and dendrites has outgrown from single transplanted neurons with appreciable density of axonal boutons and dendritic spines throughout their length (Fig. 1F, insets, and movie S1).

As spontaneous cell-to-cell fusion events can occur between transplanted cells and central nervous system neurons, although these are extremely rare (*28*, *29*), we tested for the occurrence of cell fusion by using Emx1-Cre/GFP donor cells (*30*, *31*) and tdTomato reporter

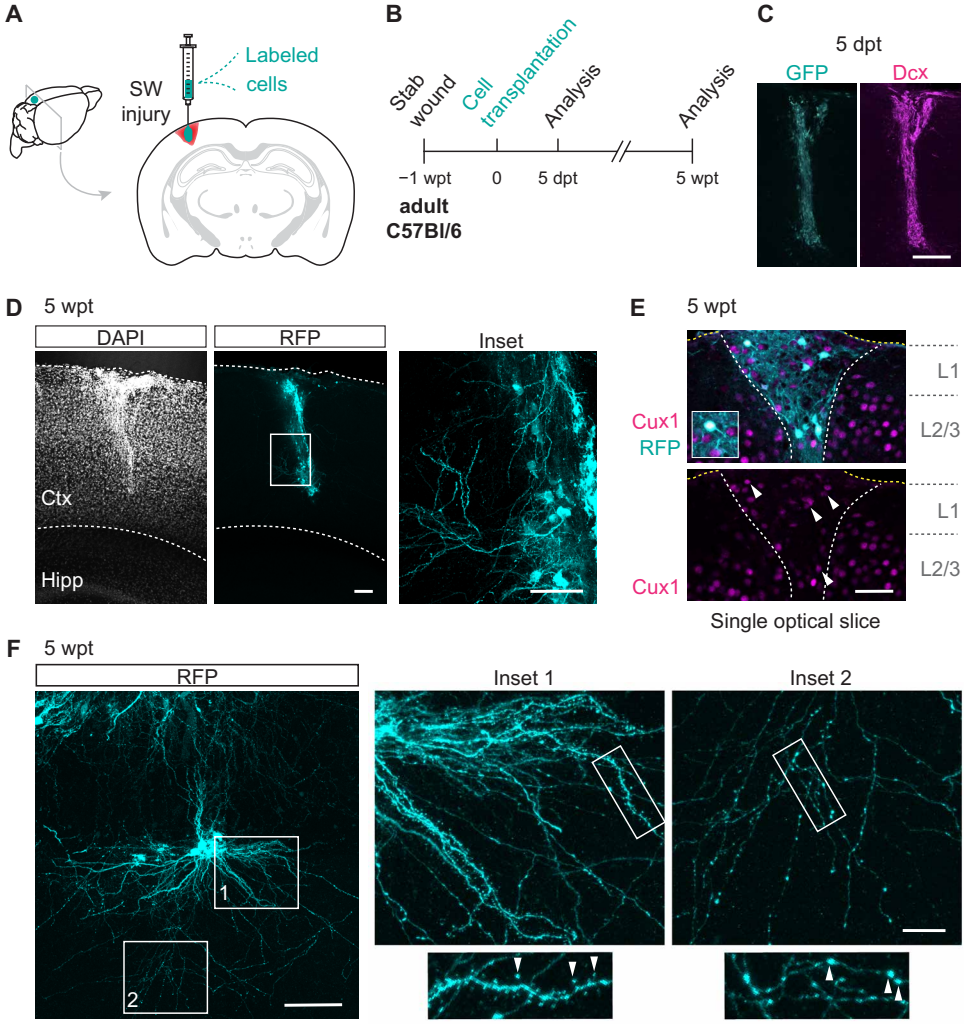

Fig. 1. Transplanted neurons develop mature morphologies and synaptic structures within a cortical stab injury. (**A** and **B**) Schematic and timeline of the experimental procedure. (**C**) Representative confocal image of a GFP graft, 5 dpt, showing an almost complete overlap with the immature neuronal marker Dcx ($n = 4$). (**D**) Confocal images of a representative transplantation site in the mouse cortex inflicted by a SW injury, 5 wpt [see all nuclei stained with 4′,6-diamidino-2-phenylindole (DAPI); $n = 5$]. The boxed area highlights dendritic branches of RFP transplanted neurons. (**E**) Example image of a single optical section in the transplant shows colocalization of RFP with Cux1, a marker of upper layer cortical identity ($n = 2$). (**F**) Z-stack projection of an example of grafted neurons and respective high-magnification insets shows the extension of apical dendrites as well as profuse basal dendrites (1) and axonal arborizations (2) from the cell bodies ($n = 5$). Notice the appearance of spines and boutons in dendrites and axons, respectively (arrowheads in the highlighted neurite). Scale bars, 100 μm (C and D, left), 50 μm (D, right; E; and F, left), and 10 μm (F, right). Ctx, cortex; Hipp, hippocampus.

mice as hosts (fig. S1A) (*32*). Cell fusion upon transplantation would result in Cre-mediated recombination and expression of tdTomato. We observed no tdTomato neurons and no GFP^+/$TdTomato^+$ neurons (fig. S1B), thus excluding cell fusion in our experimental paradigm. Together, these observations demonstrate that cells from the embryonic cortex transplanted into adult mouse cortex subjected to an invasive injury survive and develop morphological traits of mature cortical neurons, such as complex dendritic arbors and synaptic specializations.

Host environment dictates neuronal integration: Injury promotes initial integration of neuronal transplants

To uncover the synaptic network established between transplanted neurons and the host brain, we used a modified RABV that allows monosynaptic tracing of inputs to targeted cells (*33*). In this deletion mutant RABV, ΔG RABV, the glycoprotein gene (G), necessary for the trans-synaptic spread, is deleted and replaced by a fluorescent reporter. In addition, the virus envelope is EnvA-pseudotyped to infect only cells expressing TVA (avian tumor virus receptor A). As a result, the primary infection is targeted to cells coexpressing TVA receptors and the rabies G, allowing trans-complementation and assembly of new infectious particles. We therefore engineered donor cells derived from embryonic day 14 (E14) cerebral cortex cultured in vitro by retroviral infection to express RFP/G/TVA before transplantation or, alternatively, transplanted acutely dissociated cells from E18 Emx1-Cre-G/TVA/GFP embryos (*30*, *31*, *34*). Complementary GFP or mCherry-expressing ΔG RABV, injected 1 month after transplantation, thus propagates retrogradely and across one synapse to the direct presynaptic partners. As they lack G protein, infection is halted at these cells, allowing unambiguous identification and mapping at fine scale the presynaptic partners of transplanted neurons brain-wide (Fig. 2A). By combining the comprehensive anatomical registration of single cells across the entire brain with computation of the connectivity ratio (number of neurons in a given anatomical region per primarily infected neuron, also called "starter" neuron, e.g., Fig. 2B), we can run comparative analysis between connecting areas and between experimental groups (*5*). Note that every batch of RABV was tested in naïve C57BL/6J wild-type mice beforehand, and rare batches resulting in transduction of few cells in these experiments were not used in this study. Moreover, we have run in vitro controls that exclude changes in G protein levels in the transduced neurons by inflammatory stimuli, such as interferon-γ, LPS, and interleukin-1b in vitro (*35*). This is an important control because variable levels of G across conditions could result in different ability of the virus to spread and thus quantitative differences in connectivity.

To investigate whether neurons can connect properly within a gliotic microenvironment and the influence of a preceding injury, we transplanted reporter/G/TVA-expressing cells into either the SW-inflicted or intact primary visual cortex of adult mice, injected ΔG RABV (expressing a different reporter protein) 1 month later in the transplantation site, and examined the brains 1 week afterward (Fig. 2, A and C). Mapping and quantification of presynaptic input neurons showed the highest connectivity ratio for the visual cortex (primary and high-order areas) among all innervating areas in both experimental conditions (Fig. 2D; see data S1 for details). However, these short-distance connections within the visual cortex were abundant for transplants in the SW, while they were extremely scarce for neurons in the intact cortex with about eight times lower connectivity ratio (Fig. 2, D and F). In addition, the global input landscape across the brain was notably different between these conditions, with more traced input neurons per region in the SW-injured brains and with overall more connecting regions, compared to traced input neurons in the intact brains (23 versus 15 afferent regions for transplants in SW and intact cortex, respectively) (Fig. 2, D and E, and fig. S2; see table S1 for abbreviations). In both groups, transplanted neurons receive input from various cortical and subcortical regions of the ipsilateral hemisphere including sensory cortices, associative areas, and thalamic nuclei, but fewer regions are represented in the connectome of transplants in the intact cortex. A major source of inputs to the mouse primary visual cortex is the dorsal lateral geniculate nucleus (dLGN) in the thalamus, which relays visual information from the retina to the primary visual cortex (*36*). While transplants in the SW visual cortex show considerable numbers of RABV-traced input neurons from the dLGN, those in the intact group hardly do so (Fig. 2, F and G). Likewise, in the latter, contralateral connectivity is limited to a low number of input neurons in the contralateral visual cortex, whereas a few other cortical and subcortical regions of the contralateral hemisphere contribute to graft connectivity in the SW injury group (Fig. 2E). Thus, the injury condition has a profound impact on the input connectome of neuronal transplants.

To determine how close these connectomes are to the connectome of endogenous neurons in an intact cortex (naïve), we used our previously published data obtained by electroporation of upper layer visual cortex neurons with the RFP/G/TVA plasmid during mouse cortical development and subsequent RABV-mediated tracing during adulthood (*5*). Notably, the RABV strain and helper constructs, experimenter, and data analysis pipeline were the same in the present study and previous study. The overall number of afferent regions was found to be very similar with 25 regions for endogenous neurons and 23 regions for regenerated circuits after SW. However, the comparison revealed higher connectivity ratios for neurons transplanted in the SW cortex (Fig. 2E). We could appreciate a higher number of RABV-traced neurons within the visual cortex, in the neighboring retrosplenial and ectorhinal cortices, and in the distant thalamic dLGN, a key component of the visual pathway as aforementioned. In stark contrast, the connectivity of transplanted neurons in the intact brain lags significantly behind the endogenous ratios, with a local connectivity ratio about six times lower, and lower for most of the regions throughout the brain (Fig. 2E). For both groups, all the identified regions are known to project to the visual cortex (Allen Connectivity dataset) (*37*, *38*). Thus, neuronal integration into preexisting circuits of the mouse cerebral cortex requires an altered local environment, but a highly inflammatory and gliotic parenchyma is overly permissive to inputs, resulting in supernumerary graft-host connections.

Neuronal survival and differentiation in the intact cortex resemble those in injured cortex

One possibility explaining the poor input connectivity to neurons derived from transplants into the intact cortex could be poor differentiation and/or survival. To explore this, we analyzed grafts at early time points after transplantation (fig. S3A). Five days after transplantation into the intact cortex, the graft was largely immunopositive for Dcx, similarly to that observed in the SW grafts (fig. S3B and Fig. 1C). This finding suggests that the transplanted cell population goes through a similar trajectory with no major imbalance or lag in

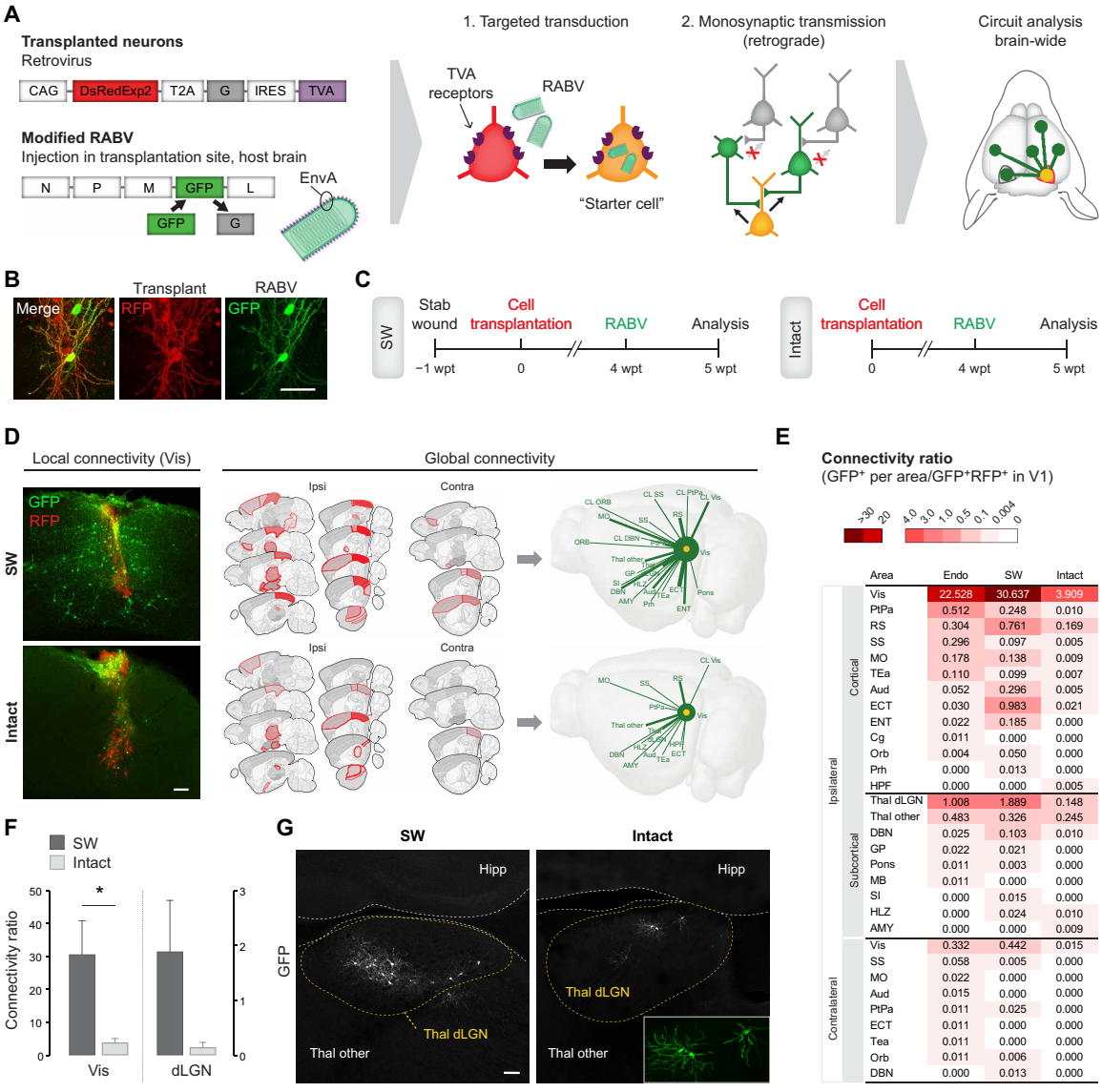

Fig. 2. Input connectivity of neuronal transplants in SW and intact cortex. (**A**) Molecular tools and rationale of brain-wide monosynaptic tracing. (**B**) Example of a starter neuron (RFP^+/GFP^+): a neuron within the RFP transplant (RFP^+) that has been infected by the GFP RABV. (**C**) Experimental timeline. (**D** and **E**) Local and brain-wide inputs (GFP-only) to transplants, traced at 4 wpt ($n = 4/5$). (D) Schematics depict brain regions that innervate the transplant. Red grading in sagittal sections and thickness of the lines in three-dimensional connectograms reflect the connectivity ratio for a given connection. (E) Color-coded connectivity ratios for transplants in SW or intact cortex ($n = 4/5$, respectively), as well as for endogenous neurons. The data shown for endogenous neurons (Endo) have been published before (*5*) and are used here solely for comparison. Note the excessive connectivity in SW and scarce connectivity in intact, as compared to the native. (**F**) Quantification of Vis-Vis and dLGN-Vis connectivity ($n = 4/5$; $^*P < 0.05$ using Mann-Whitney test). (**G**) Presynaptic neurons (GFP^+) in the dLGN of the thalamus. Scale bars, 50 μm (B) and 100 μm (D and G). See table S1 for abbreviations. Contra, contralateral; Ipsi, ipsilateral.

their differentiation. Moreover, neurons had already projected many neurites through the host parenchyma (fig. S3, B and C). These neurites display enlarged terminal structures at their tips, which were reminiscent of growth cones, suggesting ongoing pathfinding. A few had reached the corpus callosum at about 300 to 400 μm from the transplant, indicating no major obstacle to their navigation through the adult cortical tissue. By 2 wpt, spine-bearing dendrites were identifiable (fig. S4C) and neurons had acquired expression of the mature neuronal marker NeuN (fig. S4, B and C). Many coexpressed the upper layer neuron marker Cux1 as observed for transplants in an SW injury (fig. S4B and Fig. 1E; 63.47% and 70.27%, respectively) or in a neuronal ablation injury (*5*). Last, graft volume was considered as a proxy for graft survival, and no significant difference on graft volume was detected between intact and SW cortex despite a trend of the latter toward larger volumes (fig. S5). Worth noting, however, is the significant decrease in graft volume between 1 and 3 months after SW (fig. S5B). To test whether this may relate to the lower connectivity ratio, we plotted the graft volume and the connectivity ratio of the visual cortex but found no significant correlation (fig. S5, D to F). Together, these data indicate that the environment of the intact cerebral cortex can nurture early neuronal development but fails to allow adequate synaptic integration of new neurons.

LPS-elicited inflammation is insufficient to promote graft-host connectivity

One obvious difference between the intact and SW-injured cortex is the activation of glial cells and the inflammatory stimuli elicited by this invasive injury (*15*, *16*, *24*, *26*, *39*). To determine whether such an inflammatory component of an injury may be sufficient to elicit the circuit plasticity required for the adequate integration of new neurons, we injected bacterial LPS intraperitoneally, transplanted cells 1 week later, and then analyzed their connectivity. First, we monitored the reactive gliosis elicited by different LPS concentrations at 1 week after injection in comparison to the reaction elicited by the SW injury (Fig. 3A). Chosen concentrations were previously used as an inflammatory challenge (*40*–*42*) without neuronal cell death (*43*, *44*). Reactive astrocytes and microglia were stained by glial fibrillary acidic protein (GFAP) and ionized calcium binding adaptor molecule 1 (Iba1), respectively, and showed evident reactivity in the SW and with the higher LPS dose even though not the very same extent as in the penetrating stab injury (note that GFAP in LPS is not significantly higher than in the intact group despite a trend; Fig. 3, A and B). Hypertrophic astrocytes and deramified microglia were noticeable in these two groups as compared to the resting-like counterparts characterized by the lack of GFAP and thin/multiple processes, respectively, observed in the intact cortex and contralateral to SW. In contrast, immunoreactivity and glial cell morphology with the lower LPS dose was comparable to the contralateral visual cortex from SW brains or to the intact cortex (Fig. 3A).

We therefore used the higher LPS dose, eliciting stronger reactive gliosis to test the influence of inflammation in graft connectivity (Fig. 3C). Connectivity ratios of neuronal transplants in the cortex with LPS-induced reactive gliosis were rather similar to those in the intact cortex, despite a small trend for a higher local connectivity (15 versus 13 afferent regions; 6.64 versus 3.91 connectivity ratio for visual-visual connections, for the LPS and intact groups, respectively). These experiments revealed a minor or neglectable role for LPS-induced inflammation and the ensuing reactive gliosis in graft-host synaptic connectivity.

Increased levels of complement proteins and reduced levels of synapse proteins in the SW cortex

As LPS-induced inflammation showed little effect boosting the integration of the neurons differentiating in the transplants, we pursued an unbiased proteomics approach to identify mechanisms fostering integration of new neurons in the host environment. Using a biopsy punch, we collected the host visual cortex at the time when cells would normally be transplanted, i.e., 1 week after inflicting the SW injury or after LPS injection, and collected the same region from age- and sex-matched control visual cortex ("intact"; Fig. 4A). We collected the ipsilateral visual cortices of SW mice (n = 10 hemispheres, from 10 mice), both visual cortices of LPS-injected mice (n = 10 hemispheres, from 5 mice), and both visual cortices of control intact mice (n = 20 hemispheres, from 10 mice). By shotgun proteomics using liquid chromatography–tandem mass spectrometry (LC-MS/MS), we reproducibly detected a total of 5225 proteins and quantitatively compared the samples testing for significant differences (t test). First, we compared each of the conditions (SW/LPS) with the control samples (intact brain).

After SW injury, 221 proteins differed significantly in their abundance compared to the control (Fig. 4B and data S2A). A total of 168 proteins were significantly enriched in the injury condition including some expected proteins, such as GFAP (7.65-fold) and vimentin (Vim; 3.21-fold), which are up-regulated in reactive astrocytes (see Fig. 3A for GFAP) (*15*, *38*, *45*). Likewise, the typical injury-associated extracellular matrix (ECM) proteins transglutaminase 1 and 2 and inter-trypsin α inhibitors (*16*) were significantly enriched. Consistent with an ongoing inflammatory response, gene ontology (GO) term enrichment analysis for biological processes showed significantly enriched categories such as "acute inflammatory response"/"inflammatory response" and "activation of immune response" including, e.g., the complement factor C3; complement C1q subcomponent subunits A, B, and C (C1qa, C1qb, and C1qc); immunoglobulin heavy constant γ 1 (Ighg1); Ig κ constant (Igkc); α-1-acid glycoprotein 1 (Orm1); Ig heavy constant (Ighm); signal transducer and activator of transcription 3 (Stat3); and Ig γ-2B chain C region (Ighg2b) (highlighted GO terms in Fig. 4D; data S2B). We noted several complement system–related proteins, besides C3 and various C1q, like complement C4 B (C4b), complement factor b (Cfb), and complement factor h (Cfh). Together, these are involved in the classical and alternative pathways of the complement system that propagate neuroinflammation (*46*–*48*) and have been implicated in synapse and dendrite remodeling in different conditions (*18*, *46*, *49*). Accordingly, GO term enrichment analysis revealed the significantly enriched categories "complement activation" and "synapse pruning" that both include C4b, C3, C1qa, C1qb, C1qc, Cfh, Cfb, Igkc, Ighg1, and integrin α-M (Itgam), among other proteins. Consistent with the damage to the blood-brain barrier in this injury model (*50*), each of the three polypeptide chains forming the blood protein fibrinogen (fibrinogen α, β, and γ chains, i.e., Fga, Fgb, and Fgg, respectively) was significantly more abundant. Fibrinogen induces spine elimination via microglia activation in a model of Alzheimer's disease with vascular dysfunction (*51*). Fibrinogen binds the same receptor as complement protein (CR3 or CD11b) (*17*, *50*), and presumably, both ligands thus contribute to microglia-mediated synapse pruning in conditions involving a breach of the cerebral vasculature. The significant increase of fibrinogen and C1q in the SW cortex was further verified by immunostaining (fig. S6, A and B).

We also detected 53 proteins with significantly decreased abundance after SW. These included proteins known to perform a variety of central roles in maintaining cell function. Among the most down-regulated proteins are 14-3-3σ (Sfn), a protein that is highly conserved and multifunctional, regulating essential cellular processes from cell metabolism to transcription and signal transduction (*52*), and known to be down-regulated in brain disease (*53*). In addition, proteins with central roles in transcriptional regulation and part of transcription machinery, such as the histone-lysine *N*-methyltransferase (Smyd3) and the DNA-directed RNA polymerase II subunit (Polr2c or Rpb3), were found to be significantly decreased (*54*, *55*). COUP transcription factor 1 (CoupTF1 or Nr2f1), a transcription regulator that controls neurogenesis/gliogenesis balance, was found to be down-regulated in our data and in previous work upon neuroinflammation (data S2A) (*56*). Other proteins involved in neurogenesis are down-regulated such as the chromatin remodeling factors: transcription activator BRG1 (Smarca4), chromodomain-helicase DNA binding protein 5 (Chd5), and transcriptional repressor p66-β Gatad2b. Accordingly, GO terms include "histone modification," "regulation of neurotransmitter receptor activity," and "regulation of neuronal synaptic plasticity" (data S2B). The latter includes disk large homolog 4 (Dlg4), SH3 and multiple ankyrin repeat domains protein 3 (Shank3), glutamate receptor ionotropic NMDA 1

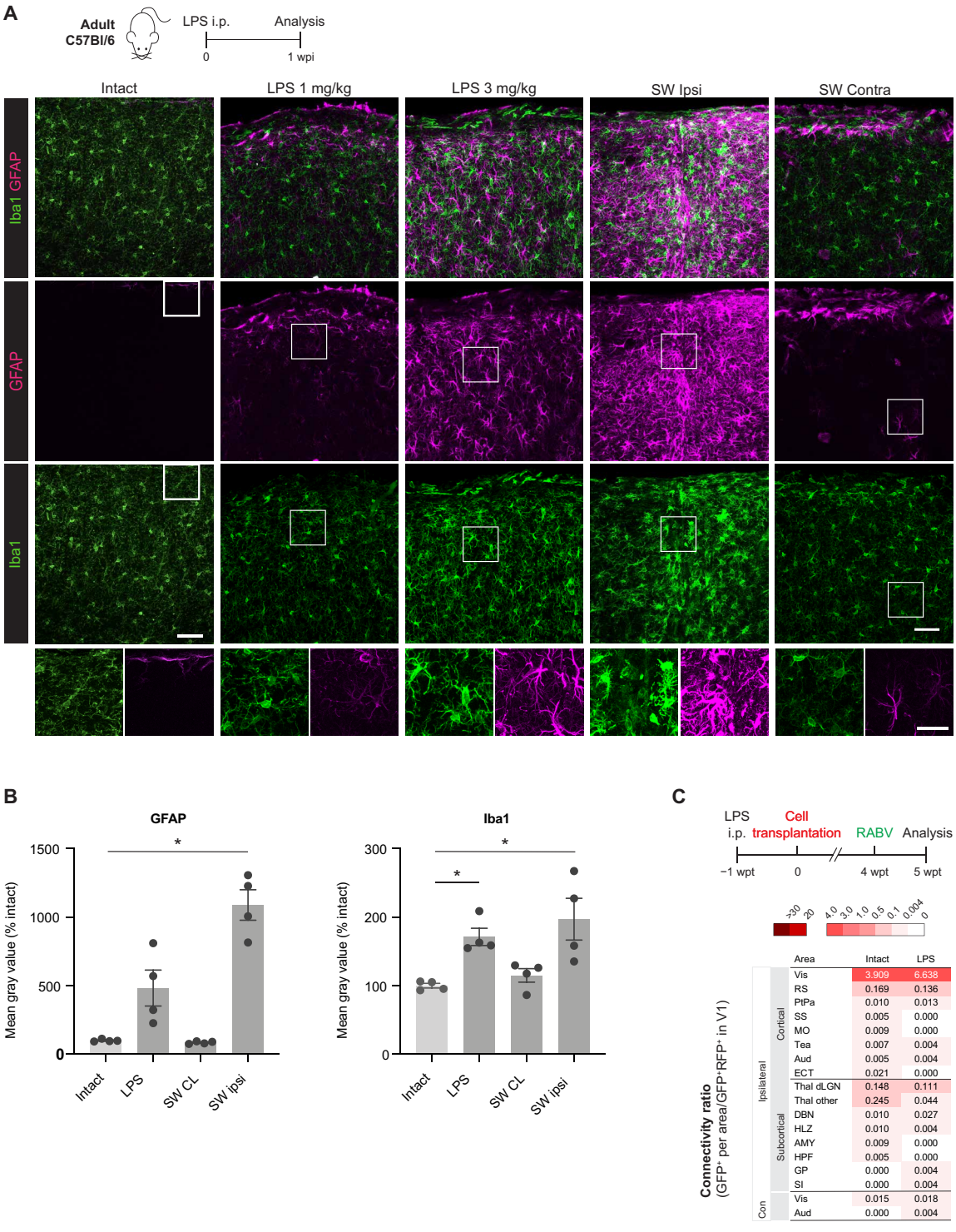

Fig. 3. Gliosis in the various experimental groups and input connectivity of neuronal transplants in LPS-induced cortex. (**A**) Timeline (top) and confocal images of the visual cortex of mice treated with LPS (1 or 3 mg/kg), or inflicted with a SW injury, and controls (intact, i.e., naïve mice and contralateral SW, as an additional control to SW). Sections were immunostained for microglia and reactive astrocyte markers (Iba1 and GFAP, respectively; bottom) [$n = 4$ for all conditions except LPS (1 mg/kg), where $n = 2$ mice were analyzed]. Note that the cellular response with the highest concentration of LPS is much closer to that observed in the SW-inflicted cortex. Insets are zoomed on the bottom row for appreciation of the differences in cellular morphology and GFAP expression. (**B**) Mean gray value of all pixels, calculated using Z-stack projections of similar thickness, for intact, LPS (3 mg/kg), and SW groups ($n = 4$; note that cortical layer 1 was excluded from the selected area). (**C**) Timeline and analysis of the brain-wide monosynaptic input to grafts in the brain of LPS (3 mg/kg)–treated mice as compared to those in the brain of intact mice ($n = 5/6$, respectively). Scale bars, 50 μm (A). See table S1 for abbreviations. Con, contralateral; i.p., intraperitoneal; wpi, weeks post-injury (SW)/ injection (LPS).

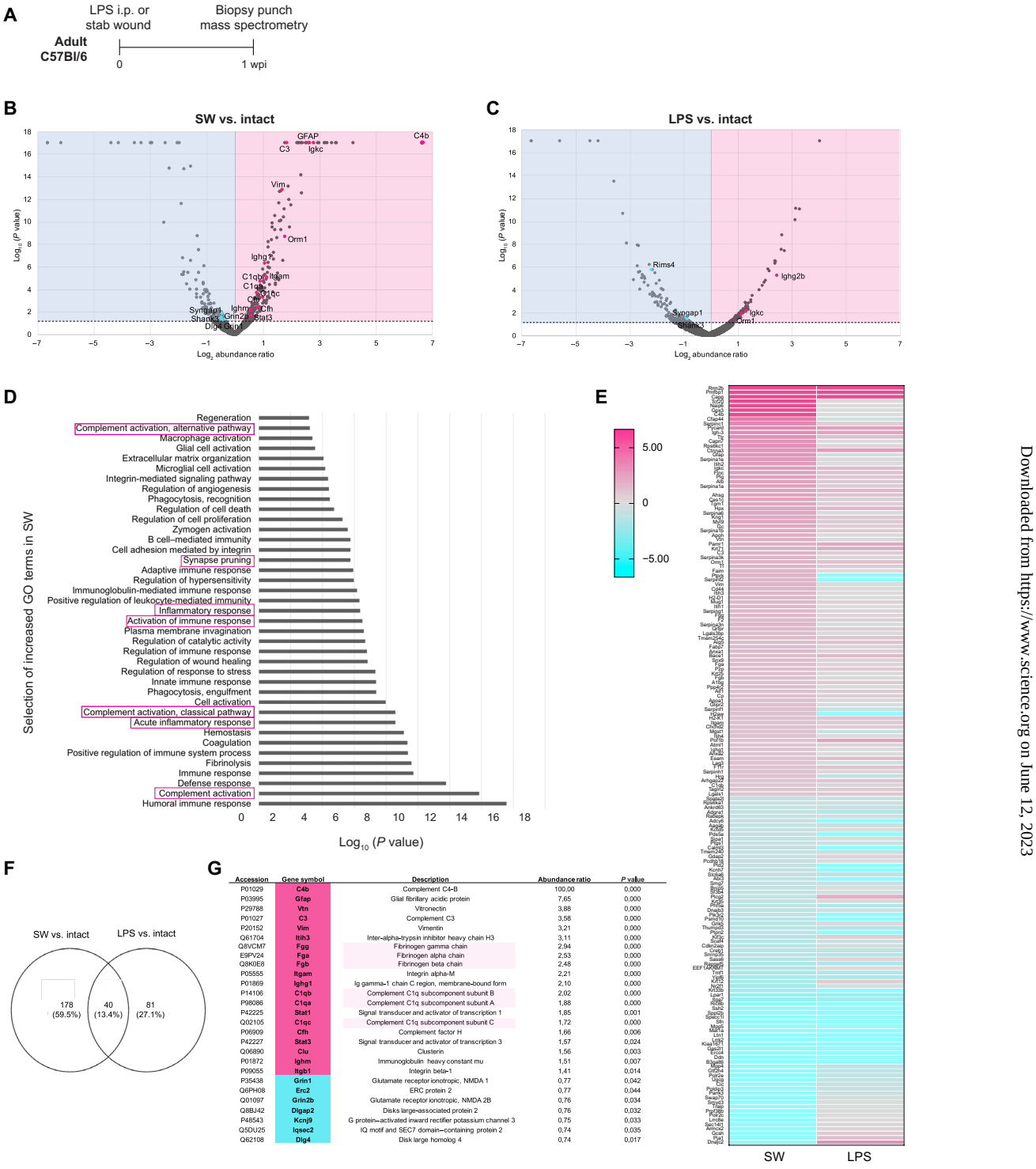

Fig. 4. Comprehensive proteome analysis of SW-injured and LPS-inflamed visual cortex. (**A**) Timeline for tissue punch collection. (**B** and **C**) Volcano plots showing $\log_2$ mean abundance ratio and corresponding $\log_{10}$ *P* value comparing SW-injured ($n = 10$) (B) and LPS-treated ($n = 10$) (C) with intact control ($n = 20$) cortical tissue (derived from 10, 5, and 10 mice, respectively, as we can consider both hemispheres from LPS and intact brains). Up-regulated proteins are in the pink area, and down-regulated proteins are in the blue area of the plots. (**D**) Selection of enriched gene ontology (GO) terms (biological process) of significantly enriched proteins in SW versus intact cortex. For the complete set of GO terms, see data S2. (**E**) Heatmap shows the significantly regulated proteins in the SW cortex, along with their regulation in the LPS cortex. (**F**) Venn diagram depicts differentially regulated proteins that overlap or are exclusive for each condition. (**G**) Selection of proteins that are exclusively up- or down-regulated in the SW-injured cortex. Highlighted are proteins further tested by immunostaining (see fig. S5). See data S2 for protein and GO analysis. wpi, weeks post-injury (SW)/injection (LPS).

and NMDA 2b (Grin1 and Grin2b), and Ras/Rap guanosine triphosphatase–activating protein (Syngap1), suggesting a decrease of synaptic structures after brain injury (Fig. 4B and data S2, A and B). These data are consistent with reduced neuronal excitability and firing in the acute phase after TBI (*57*).

Comparing the LPS-induced cortex biopsies to controls, we found 123 proteins of significantly different abundance (Fig. 4C and data S1C). Among the 60 proteins more abundant upon LPS injection, we observed Ighg2b, Igkc, and Orm1, similar to the increased proteins in the brain injury. We also found the increased GO term "acute inflammatory response" to be enriched in LPS condition (data S2D). Among the 63 proteins with lower abundance, e.g., Sfn is similarly on the three most down-regulated, and also synapse-related proteins like Shank3, Syngap1, and regulating synaptic membrane exocytosis protein 4 (Rims4), suggesting some, albeit small (Fig. 4E), overlap and similarity between SW and LPS conditions.

We next focused on the proteins uniquely regulated upon SW and not upon LPS, as they may contribute to fostering the integration of new neurons (Fig. 4, E to G, and data S2E). The activation of the complement system, synapse pruning, and immune system proteins like C4b, C3, C1qa, C1qb, C1qc, Itgam, and Ighg1 were specific to this environment, as was the enrichment of GFAP, Vim, Fga, Fgb, and Fgg. Immunostaining for C1q and fibrinogen showed no difference in signal intensity between intact and LPS cortex corroborating these results (fig. S6, A and B). In addition, the down-regulated proteins Dlg4, Grin1, Grin2b, and others that are involved in synaptic plasticity were injury-specific.

Together, proteome comparison of microenvironments eliciting low and high graft connectivity reveals fibrinogen and complement activation as possible mechanisms that may promote integration of new neurons into synaptic networks of the host brain. At the same time, these findings led us to ask whether their integration is stable or synapse pruning lingers for a longer period and eventually affects also newly formed host-graft connections.

Excessive number of input neurons in cortical stab injury is transient

Given the above observation that fibrinogen and complement factors are particularly abundant in the SW condition, and their documented role in synaptic pruning, we set out to determine the persistence of new synapses after the initial synaptic integration in this condition. In the neuronal ablation model, we had observed a net increase in spine number in the first month, followed by one more month of active spine turnover with no overall change in input connections and a stable connectivity ratio between 1 and 3 months post-transplantation (mpt) (*5*). We therefore traced input connectivity at 3 mpt in SW cortex and compared to the data obtained at 1 mpt (Fig. 5A). Unexpectedly, by 3 months, the number of RABV-traced input neurons was severely diminished, with about threefold fewer traced neurons locally (Fig. 5, B and C) and a total of 13 afferent regions as opposed to the earlier 23 (Fig. 4, C and D). Connectivity had dropped to metrics below those of normal circuits (endogenous connectivity), with only 5 as compared to 12 afferents with connectivity ratio $\geq$ 0.05. Most of the regions with few traced neurons (connectivity ratio $\leq$ 0.03) observed at 1 mpt had been lost, with, e.g., only one contralateral innervation persisting, from the contralateral visual cortex. Although the calculated connectivity ratio accounts for the number of starter neurons, note that grafts at later time points were overall smaller (fig. S5B), suggesting that not only loss of synapses but also cell death has occurred between 1 and 3 mpt. This is a notable difference from other conditions, such as in the brains with targeted neuronal ablation (*5*). These results imply profound changes in the input connectome and highlight the need to explore specific injury conditions before the use of transplants for neuronal replacement therapy.

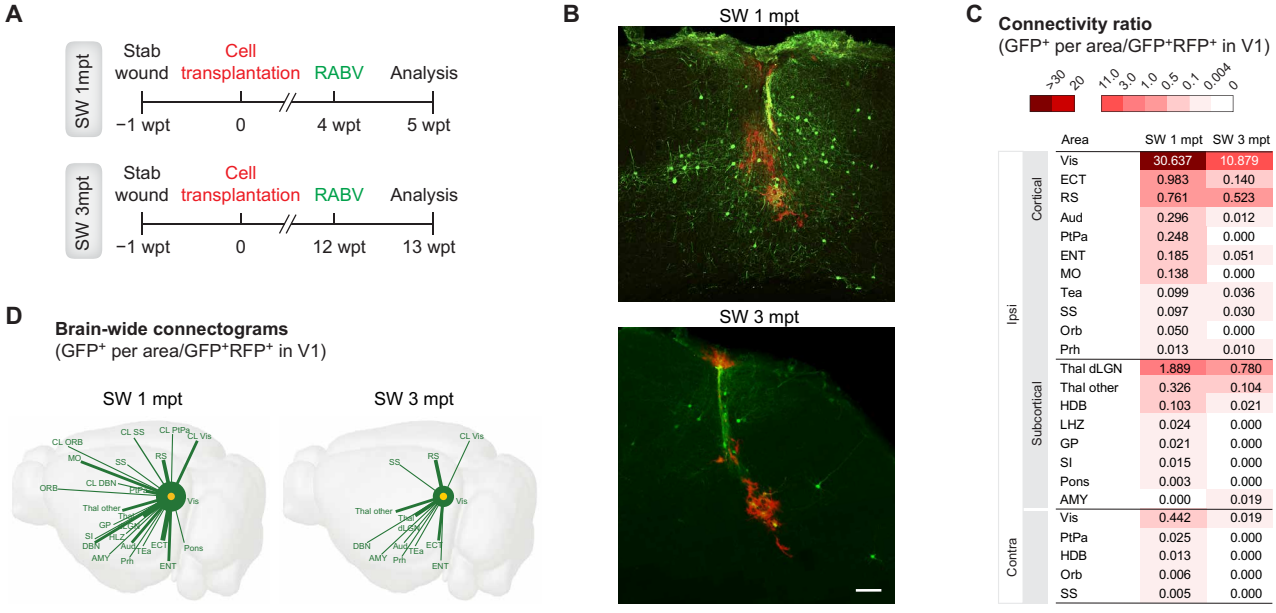

Fig. 5. Comparison of early and late connectivity shows transience in cortical stab injuries. (**A**) Experimental timelines. (**B**) Local inputs (GFP-only) to transplants, traced at 1 and 3 mpt. (**C**) Color-coded brain-wide connectivity at 1 or 3 mpt in SW ($n = 4/6$, respectively). Decreased connectivity at 3 mpt shows that many of the early synaptic connections have been pruned. (**D**) Distribution and strength of single host-graft connections evidenced by the thickness of the lines between the graft (yellow) and each area (green). Scale bar, 100 μm (B). See table S1 for abbreviations.

DISCUSSION

Despite the broad experimental use of neuronal transplantation for cell replacement in cortical brain injury, an outstanding open question is still whether the injured environment, variable across pathologies, plays a role in the integration of transplanted neurons into preexisting circuits. Our data show that the RABV-traced input connectome of transplanted neurons is highly influenced by the local environment where they develop. While the transplant survival and gross morphological maturation share features across different host environments, its degree of input connectivity with the host circuits and stability of these new connections differs substantially in the time points monitored here.

By transplanting the same donor cell type as previously in a neuronal ablation model (*5*) now in a penetrating TBI, we demonstrated pronounced differences in initial and long-term input connectivity, with initial abundant numbers of traced input neurons that were eventually reduced to subnormal levels. In contrast, neurons grafted in intact or LPS-induced networks were scarcely innervated by only few RABV-traced neurons in the host brain. However, we cannot exclude that this low number of input neurons would normalize at later stages, although we consider this unlikely given the relatively stable environment later on.

Neurons derived from mouse embryonic stem cells fail to project long-distance axons after transplantation if no injury is previously inflicted, as opposed to an injured brain, despite good graft survival in both experimental groups (*58*). Transplantation into the intact dentate gyrus or striatum of adult immunodeficient Rag2$^{-/-}$ mice yielded widespread inputs to large transplants, but their quantitative nature is unknown (*59*). Cells from the spinal cord of rat embryos transplanted into the adult rat spinal cord fail to contact nearby corticospinal axons if no spinal cord injury precedes (*60*). In addition, transplantations of embryonic neurons in the postnatal mouse cortex have suggested that a preceding apoptotic injury promotes morphological maturation and synapse formation between the host and graft (*61*). There are obstacles to the development of graft outputs and inputs in the intact central nervous system. Our findings add knowledge by showing a priming effect of an injury opening brain networks to accommodate new neurons and form new synapses in the adult cerebral cortex. On the flipside, it now became obvious that not all injuries lead to the same level of host-graft connectivity in the long term.

Several previous studies have shown that neuronal grafts in the injured postnatal or adult rodent cortex receive inputs from the host brain (*5*, *6*, *13*, *58*, *61*). However, a comprehensive comparison of the connectivity levels with native circuits has been a more challenging endeavor addressed by only a few studies (*5*, *6*). On the basis of our findings here using the SW injury, we could hypothesize that an excessive input is also observed in transplants developing in another inflammatory condition like stroke. However, using a semiquantitative analysis, Tornero *et al.* (*6*) have reported input connectivity that resembles the normal circuitry when quantifying the contribution from each input region in three categories. This quantification may not resolve all the differences we found here. In addition, possible differences may be attributable to several reasons. First, transplantation of human induced pluripotent stem cell (iPSC)–derived neurons requires immunosuppression and hence alters the environment. Second, the time and site of transplantation differs because the authors grafted iPSC-derived cortically fated neurons nearby the stroke area and only 48 hours after the stroke (compared to 1 week post-injury in our study) when microglia numbers and reactivity at the site of transplantation is peaking and thus synapse pruning may be exaggerated, leaving the initial connectome at lower metrics. Third, the degree of maturation differs profoundly with a much slower maturation speed of human neurons that are still rather immature at the time of RABV injection (2 mpt; only 20% NeuN) (*62*), and thus, the mapped connectivity may be a premature assessment of an expanding connectome. Data from brain imaging and network neuroscience have been converging into the view that TBI is characterized by an increased endogenous connectivity, while the transience of this hyperconnectivity is still under debate (*63*). Slicing the brain also correlates with a substantial, rapid increase in synapse number compared to tissue fixed in vivo (*64*). However, stroke differs in many parameters from TBI and may hence influence connectivity differently, highlighting the need to examine quantitative connectivity specifically in different injury conditions. This is also confirmed by our accompanying manuscript (*35*), showing the influence of the aging brain and amyloid-loaded host environment in promoting the input connectome locally.

Our data showed a sharp decline in the number of RABV-traced neurons in the SW cortex at 3 mpt. Two models fit this observation. One scenario is that excessive synaptic pruning leads to a net loss of synapses between host and graft. Another scenario is a refinement of the number of input neurons to fewer neurons, each making more synaptic connections with the graft, which would result in the same reduction of traced input neurons. These possibilities can only be discerned by spine analysis and electrophysiology and paired recordings, which is important to pursue.

It is difficult to compare our above described findings with transplants of human PSC-derived neurons, as these mature at a very different pace and develop in an immunosuppressed environment. However, previous work showed an unexpectedly early innervation already at 1.5 to 2 mpt after transplantation that is comparable at more mature stages at 6 mpt, in stroke and Parkinson's disease models (*6*, *7*). It will be intriguing to analyze these transplants at even later stages, given the slow pace of human neuron maturation (*65*, *66*).

Analysis of the proteome from environments that promote graft connectivity (SW) as compared with those where transplant connectivity remains under normal levels (intact/LPS) suggests that fibrinogen and complement activation pathways play a role in synapse yield. Both have been implicated in synapse pruning during brain development and/or neurological disease, namely, in TBI (*18*, *46*, *51*, *67*). Gene expression analysis in the neuronal apoptosis model, where we have previously observed an adequate and stable level of connectivity, showed all the three components of C1q (C1qa, C1qb, and C1qc) differentially overexpressed in injured regions (*8*). Collectively, our findings indicate that complement protein levels and its temporal dynamics at a brain injury may play an essential role, dictating the outcome of transplantation and stability of new synaptic connections.

Successful brain repair by cell transplantation involves not only axonal outgrowth and generation of new synapses with the correct regions but also a tight quantitative match of the new input and output connections. In the mammalian cortex, excessive excitatory connections may result in hyperexcitability and formation of epileptic foci in the transplanted site, while scarce connections may be insufficient to restore the functional deficit caused by the injury. Here, we provide the first evidence that injury type–dependent extrinsic cues influence the integration of transplanted neurons into

the host synaptic circuitry, specifically, their afferent connectivity. Future research is needed to investigate the functional relevance of the inputs mapped here, or in another model of acute brain injury, such as stroke. This work further advances our understanding of the prerequisites for neuronal replacement in damaged brain circuits and represents an important step in clinical translation of neuronal replacement strategies to restore an authentic circuitry after brain damage and promote functional recovery in the injured brain.

MATERIALS AND METHODS

Experimental design

Animals

Animal handling and experimental procedures were performed in accordance with German and European Union guidelines and were approved by the Government of Upper Bavaria. All efforts were made to minimize suffering and number of animals. Both male and female mice were used. Mice were kept in specific pathogen–free conditions and in 12-hour:12-hour light/dark cycles with food and water ad libitum.

All mice were 2 to 4 months old at the time of the first surgery. C57BL/6J wild-type mice were used as host mice for all studies except those to test for the occurrence of cell fusion wherein tdTomato reporter mice were used (Ai9) (*32*). Surgeries were performed aseptically under anesthesia with a mixture of fentanyl (0.05 mg/kg; Janssen), midazolam (5 mg/kg; Roche), and medetomidine (0.5 mg/kg; Fort Dodge). After surgery, anesthesia was terminated with atipamezol (2.5 mg/kg; Janssen), flumazenil (0.5 mg/kg; Hexal), and buprenorphine (0.1 mg/kg; Essex). Meloxicam (1 mg/kg; Metacam) was administered for postoperative analgesia.

Cells for transplantation were obtained from C57BL/6J wild-type or Emx1-Cre/EGFP E14.5/E15.5 mouse embryos (*30*, *31*) and cultured (see below), or alternatively, they were mechanically dissociated from E18.5 Emx1-Cre/G-TVA/GFP embryos (*30*, *31*, *34*) and readily transplanted. Triple transgenic embryos amid the litter were identified by GFP expression in the dorsal telencephalon and resulted from matings involving a G-TVA homozygous parent.

Cell cultures

Primary culture of cortical neurons. Neocortex from E14.5/E15.5 mouse embryos was mechanically dissociated in Hanks' balanced salt solution buffered with 10 mM Hepes (both from Life Technologies). Cells were plated in poly-D-lysine (20 μg/ml; Sigma-Aldrich)–coated 24-well plates at a density of 200,000 cells per well. Cells were initially kept in 10% fetal bovine serum (FBS; PAN-Biotech)–containing high-glucose Dulbecco's modified Eagle's medium (DMEM) (4.5 g/liter) with GlutaMAX plus penicillin-streptomycin (both from Life Technologies). Serum was gradually removed by replacing half of the medium with B27 (Life Technologies)–containing high-glucose DMEM (4.5 g/liter) with GlutaMAX plus penicillin-streptomycin on each of the following 2 days. Cells were harvested for transplantation after 4 to 5 days in vitro upon validation of reporter expression.

All cells for primary culture were obtained from wild-type C57BL/6J mice except those used to test for the occurrence of cell fusion with the host cells. For this purpose, Emx1-Cre/EGFP (*30*, *31*) embryos were used. Double transgenic embryos amid the litter were identified by GFP expression in the dorsal telencephalon.

Virus treatment in cell cultures

Neocortical neurons from C57BL/6J wild-type mouse embryos were cultured. Two to 4 hours after plating, the cells were transduced with MMuLV (moloney murine leukemia virus)-derived retroviral vectors CAG-EGFP or CAG-DsRedExpress2-2A-Glyco-IRES2-TVA (0.8 to 1 μl per well; titers ranged from 10^7 to 10^{11} transducing units/ml). Cells were then transplanted into C57BL/6J wild-type adult mice. For cell fusion test experiments, neuronal cultures were prepared from Emx1-Cre/EGFP E14.5/E15.5 embryos and transplanted into tdTomato reporter mice. Although these cells are endogenously labeled, we additionally treated them with CAG-EGFP retrovirus to account for a putative impact of retroviral transduction in the propensity of cells to fuse upon transplantation in the adult brain parenchyma.

Treatments and surgical procedures

LPS inflammatory stimulus. C57BL/6J wild-type mice were subjected to an inflammatory stimulus by a single intraperitoneal injection of LPS (1 or 3 mg/kg) from *Escherichia coli* (Sigma-Aldrich). A batch of mice was used to run a comparative analysis of cortical gliosis in SW, LPS, and control conditions. For this purpose, a craniotomy was performed at the time of the LPS injection to account for glial reactivity due to the craniotomy per se. These mice were perfused 7 days after the LPS treatment to monitor cortical gliosis at the time when transplants would normally be performed. Other mice were used for subsequent neuronal transplantation and connectivity analysis (see below).

SW injury. C57BL/6J wild-type or tdTomato reporter mice were used for cortical SW injury as described by Mattugini *et al.* (*26*). Briefly, mice were anesthetized and a craniotomy of 2.5 mm diameter was open to expose the primary visual cortex (V1) of the left cortical hemisphere. Using an ophthalmological lancet, a 0.5-mm-deep/1-mm-long incision was performed within V1 borders (coordinates from lambda: 0.0 ± 0.2 anteroposterior and 2.0 ± 0.2 to 3.0 ± 0.2 mediolateral; coordinates were chosen to avoid large pial vasculature). The bone flap was placed back, and the skin was sutured. For analysis of cortical gliosis, mice were perfused 7 days after SW, while for analysis of graft integration the mice were subjected to further surgical procedures (see below).

Cell transplantation. Cells were transplanted unilaterally into one V1 of the mouse cerebral cortex. Host mice belonged to three groups: SW, intact (naïve), and mice subjected to an inflammatory stimulus by intraperitoneal injection of LPS (3 mg/kg). Transplantation into SW or LPS mice was performed 7 days after the respective insult. In SW group, donor cells were placed right into the center of the incision, still lightly visible.

Donor cells were fluorescently labeled in Emx1-Cre/EGFP or Emx1Cre/G-TVA/EGFP mouse lines or via in vitro viral transduction with the aforementioned constructs. Cultured cells were washed three times with prewarmed phosphate-buffered saline (PBS) to remove any remaining viral particles and cell debris. Gentle trypsinization (0.025%; 10 min at 37°C) detached the cells, and trypsin was then inactivated by FBS-containing medium (1:1). The cell suspension was then prepared in B27-containing high-glucose DMEM (4.5 g/liter) with GlutaMAX plus penicillin-streptomycin. Donor cells (25,000 to 50,000) were transplanted in a total volume of 1 μl of cell suspension using a ga33 Hamilton syringe (coordinates from lambda: 2.5 ± 0.2 mm mediolateral and 0.0 ± 0.2 mm anteroposterior). Cell deposits were distributed dorsoventrally filling up a depth between 0.5 and 0.2 mm that results in a cellular graft encompassing cortical layers 1 to 4/5. Injection coordinates and pattern of pial vasculature were noted for later identification of the transplantation site and injection of the RABV. The bone lid was repositioned, and the skin was sutured. For analysis of transplanted neurons' survival and early

differentiation, some mice were perfused 5 days afterward, while for analysis of neuronal integration mice were subjected to RABV injection as detailed next.

RABV injection. We used retrograde monosynaptic tracing with a modified RABV (EnvA-pseudotyped ΔG-EGFP or ΔG-mCherry, complementary to the reporter in transplanted cells) (*5*, *33*) to map brain-wide synaptic input to grafted neurons. In short, the RABV was injected 1 or 3 months after cell transplantation, in three locations surrounding the transplantation site (200 nl per location), using an automated nanoinjector at a slow delivery speed. RABV titers typically ranged between 1.5×10^8 and 3.5×10^8 plaque-forming units/ml. Mice were sacrificed 7/8 days later for immunostainings and circuit analysis.

Immunostaining

Mice were deeply anaesthetized with ketamine (100 mg/kg) and xylazine (10 mg/kg) and perfused transcardially with PBS (5 min) followed by 4% paraformaldehyde (PFA) in PBS for 30 to 40 min. Brains were collected and postfixed in 4% PFA overnight, at 4°C, and serially cut on a vibratome into 70-μm sagittal sections, and slices were further processed as free floating. Sections were washed and incubated in blocking and permeabilizing solution for 2 hours (2 to 3% bovine serum albumin or 10% normal goat serum and 0.5% Triton X-100). The following primary antibodies were then used: chicken anti-GFP (1:1000; Aves Labs), rabbit anti-RFP (1:1000; Rockland), goat mCherry (1:200; Sicgen), rabbit anti-Cux1 (1:200; Santa Cruz Biotechnology), guinea pig anti-Satb2 (1:250; Synaptic Systems), mouse anti-GFAP (1:1000; Sigma-Aldrich), rabbit anti-Iba1 (1:500; Wako), rabbit anti-Dcx (1:1000; Abcam), guinea pig anti-Dcx (1:1000; Merck), mouse anti-NeuN (1:200; Merck/Millipore), sheep anti-fibrinogen (1:100, Biomol), and rabbit anti-C1q (1:1000; Abcam) for overnight to 48 hours of incubation, at 4°C. After washing, sections were incubated with appropriate species- and subclass-specific secondary antibodies conjugated to Cy3 or Cy5 (Dianova) or Alexa Fluor 488 or 647 (Invitrogen), used at 1:500 or 1:1000 depending on high (>1:500) or low (<1:500) concentration of the primary antibody. Sections were incubated for 10 min with 4′,6-diamidino-2-phenylindole (DAPI, 1 μg/ml; Sigma-Aldrich) for nuclear labeling and mounted on glass slides with Aqua-Poly/Mount (Polysciences).

For connectivity analysis, brain-wide, all sections were immunostained for GFP/RFP. For some brains, sections with the transplant were selected and subsequently stained for Cux1 colocalization analysis, and all were mounted for microscopy and serial analysis.

Slice processing and imaging

For brain-wide connectivity analysis, brain sections were kept in serial order throughout their processing. Sections with one or more GFP (or mCherry)–labeled cell somas were scanned using an epifluorescence microscope with a motorized stage (Zeiss, Axio Imager M2) equipped with a 10× objective [numerical aperture (NA) 0.3]. Automated scanning, tile alignment, and image stitching were performed to create a high-resolution image of the whole section. In sections with unclear cell numbers due to close apposition of two GFP (or mCherry) cell bodies or with high densities of GFP (or mCherry) cells, scanning of Z-stacks in a laser scanning confocal microscope (Zeiss, LSM 710) with a 40× objective (NA 1.1) was carried out. For all immunofluorescence studies, images were acquired using an epifluorescence microscope with a motorized stage (Zeiss, Axio Imager M2) and a laser scanning confocal microscope (Zeiss, LSM 710).

Mass spectrometry

Three- to 4-month-old male and female C57BL/6J mice ($n = 10$ intact controls, $n = 10$ SW-injured, and $n = 5$ LPS-injected) were sacrificed through cervical dislocation, and brains were removed and placed into cold PBS. Biopsy punches (2.5 mm diameter) of the visual cortex of both hemispheres were dissected, whereas meninges and white matter were carefully taken off. The contralateral (uninjured) cortices of the SW-injured brains were not considered for proteome analysis (intact cortical tissue: $n = 20$; SW: $n = 10$; LPS: $n = 10$). Samples were placed into low protein–binding Eppendorf tubes, frozen on dry ice, and stored at −80°C until further processing.

Tissue samples were lysed in NP-40 buffer [1% NP-40 in 10 mM tris (pH 7.4) and 150 mM NaCl] in a Precellys homogenizer (VWR), and 10 μg of total protein per sample was proteolyzed with Lys-C and trypsin using a modified FASP (filter-aided sample preparation) procedure (*68*).

LC-MS/MS analysis was performed on a Q Exactive HF mass spectrometer (Thermo Fisher Scientific) online coupled to a nano-RSLC (reverse phase liquid chromatography) (Ultimate 3000 RSLC, Dionex). Tryptic peptides were accumulated on a nano trap column (Acclaim PepMap 100 C18; 5 μm, 100 Å, 300 μm inner diameter by 5 mm; Thermo Fisher Scientific) at a flow rate of 30 μl/min followed by separation by reversed-phase chromatography (μPAC column; 200 cm length; with pillar array backbone at interpillar distance of 2.5 μm; PharmaFluidics) using a nonlinear gradient for 240 min from 3 to 42% buffer B [acetonitrile/0.1% formic acid (v/v) in high-performance LC (HPLC)–grade water] in buffer A [2% acetonitrile/0.1% formic acid (v/v) in HPLC-grade water] at a flow rate of 300 nl/min. MS spectra were recorded at a resolution of 60,000 with an AGC (automatic gain control) target of 3×10^6 and a maximum injection time of 50 ms, at a range of 300 to 1500 mass/charge ratio (m/z). From the MS scan, the 10 most abundant ions were selected for HCD (higher energy collisional dissociation) fragmentation with a normalized collision energy of 27, an isolation window of 1.6 m/z, and a dynamic exclusion of 30 s. MS/MS spectra were recorded at a resolution of 15,000 with an AGC target of 10^5 and a maximum injection time of 50 ms.

Statistical analysis

General image analysis and statistics

Images were analyzed with ZEN (Zeiss) and ImageJ software. Cell countings were performed with the Cell Counter plug-in for ImageJ by careful inspection across serial optical sections (spaced at 1-μm interval) of confocal Z-stacks acquired with a 40× objective (NA 1.1). Image processing was performed with ImageJ after stitching in Imaris Stitcher (9.6.0; Bitplane) when needed, and multipanel figures were assembled in Adobe Photoshop/Illustrator (Adobe Systems).

Statistical analysis was performed using GraphPad Prism version 8.0 software (GraphPad). All biological replicates (n; mice) are derived from at least two independent experiments (see figure legends for details on each experiment). Values are reported as means ± SEM calculated between different mice. Statistical significance was defined at $^*P < 0.05$, $^{**}P < 0.01$, $^{***}P < 0.001$, and $^{****}P < 0.0001$, except for the correlation analysis (fig. S5, D to F), where $^*P < 0.0332$, $^{**}P < 0.0021$, $^{***}P < 0.0002$, and $^{****}P < 0.0001$. For comparison of connectivity ratio, % Cux1 cells, or graft volume between conditions, nonparametric Mann-Whitney or Kruskal-Wallis one-way analysis of variance tests were used for two or more groups, respectively. For correlation analysis, the data were computed

using nonparametric Spearman correlation. Data visualization leveraged Microsoft Excel, GraphPad Prism version 8.0, and Adobe Illustrator 2020.

Statistical significance for the proteomics experiment was ascertained using the approach described in (*69*), which is based on the presumption that we look for expression changes of proteins that are just a few in comparison to the number of total proteins being quantified. The quantification variability of the nonchanging "background" proteins can be used to infer which proteins change their expression in a statistically significant manner. Proteins with $P < 0.05$ were considered significantly changed.

Connectivity analysis

Whole-slice tile scans were used to identify brain regions with GFP (or mCherry)–labeled cells by alignment with the corresponding sections of the Allen Reference Atlas of the adult mouse brain (version 2; 2011; Allen Institute for Brain Science). Some sections of interest are not available in this reference atlas, namely, in the sagittal atlas, which displays 21 sections spaced at 200-μm intervals and only up to 4.0 mm lateral from bregma. In these cases, the Brain Explorer 2 software (Allen Institute for Brain Science) was used to retrieve the corresponding annotated section and to overlap it with the experimental section to identify the anatomical location of the labeled cells. In sections with unclear cell numbers, analysis of the confocal Z-stacks was carried out, and quantification was performed by careful inspection through serial optical sections spaced at 1-μm interval. In sections including transplanted cells, four categories were considered for counting: GFP only (or mCherry only) with neuronal morphology, GFP only (or mCherry only) with glial morphology, RFP/GFP (or GFP/mCherry) cells with neuronal morphology so-called starter neurons, and RFP/GFP (or GFP/mCherry) cells with glial morphology. Connectivity ratio for a given anatomical region was calculated by computing the ratio of the total number of GFP-only cells with neuronal morphology counted in that region and the total number of GFP/RFP cells with neuronal morphology in V1, the "starter cells" (or mCherry-only neurons in a region per number of starter GFP/mCherry neurons in V1). Results are represented as means ± SEM calculated between different mice.

Important technical considerations of this system relate with intragraft connectivity. Note that a few double-labeled cells may have acquired the RABV via a synapse with another transplanted cell, instead of being primarily infected. However, as these express the rabies G, they are also starter neurons that propagate the virus brain-wide, and thus, this aspect does not interfere with our analysis. Moreover, because of a transduction rate in vitro lower than 100%, some transplanted cells are unlabeled. In case these cells innervate a starter cell, they will be labeled GFP and accounted for in the "Vis" connectivity. A minority of the GFP-only presynaptic cells counted in the full visual area are within the transplant and thus neglectable, as it can be appreciated in Figs. 2D and 5B. Note that the graft is only 250 to 300 μm in diameter, while the visual cortex is about 2.5 mm wide (mediolateral) and 2.5 mm long (anteroposterior).

Proteomic data processing—Label-free quantification

The individual raw files were loaded to the Proteome Discoverer 2.4 software (Thermo Fisher Scientific; version 2.4.1.15), allowing for peptide identification and label-free quantification using the Minora node. Database search was performed using SEQUEST HT as the search engine in the Swiss-Prot database, taxonomy mouse (17,038 sequences) with the following search settings: 10 parts per million of precursor tolerance, 0.02 Da of fragment tolerance, full tryptic specificity, two missed cleavages allowed, carbamidomethyl on cysteine as fixed modification, deamidation of glutamine and asparagine allowed as variable modifications, as well as oxidation of methionine and Met-loss combined with acetylation at the N terminus of the protein. Carbamidomethylation of Cys was set as a static modification. The Percolator node was used for validating peptide spectrum matches and peptides, accepting only the top-scoring hit for each spectrum, and satisfying a false discovery rate (FDR) of <1% (high confidence). Protein groups were additionally filtered for an identification FDR of <5% (target/decoy concatenated search validation). The final list of proteins complied with the strict parsimony principle.

Peak intensities [at RT (retention time) apex] for the top three unique peptides were used for pairwise ratio calculations. Abundance values were normalized to the total peptide amount to account for sample load errors. The protein abundances were calculated, summing the abundance values for admissible peptides. The final protein ratio was calculated using median peptide ratios of at least 10 biological replicates each (20 replicates intact, 10 replicates SW, and 10 replicates LPS). *P* values were calculated on the basis of the approach described (*69*). Data were filtered to ensure direct identifications (not based on match-between run) in at least 30% of samples within at least one experimental group. To visualize the data, volcano plots with $\log_2$ abundance ratios of sample replicates of SW and LPS versus intact control and the corresponding $\log_{10}$ *P* values were created with Microsoft Excel. For GO enrichment, significantly differentially expressed up- or down-regulated proteins were run against a background list of all detected proteins using the webserver GOrilla (http://cbl-gorilla.cs.technion.ac.il/) (*70*). A heatmap of all significantly regulated proteins of the SW condition was created with GraphPad Prism version 8.0 by plotting all significantly regulated proteins in SW condition, and subsequently, these were aligned with the corresponding proteins of the LPS condition.

SUPPLEMENTARY MATERIALS

Supplementary material for this article is available at https://science.org/doi/10.1126/sciadv.abg9445

View/request a protocol for this paper from *Bio-protocol*.

REFERENCES AND NOTES

1. R. A. Barker; TRANSEURO consortium, Designing stem-cell-based dopamine cell replacement trials for Parkinson's disease. *Nat. Med.* **25**, 1045–1053 (2019).
2. S. Grade, M. Götz, Neuronal replacement therapy: Previous achievements and challenges ahead. *NPJ Regen. Med.* **2**, 29 (2017).
3. I. Espuny-Camacho, K. A. Michelsen, D. Linaro, A. Bilheu, S. Acosta-Verdugo, A. Herpoel, M. Giugliano, A. Gaillard, P. Vanderhaeghen, Human pluripotent stem-cell-derived cortical neurons integrate functionally into the lesioned adult murine visual cortex in an area-specific way. *Cell Rep.* **23**, 2732–2743 (2018).
4. S. Palma-Tortosa, D. Tornero, M. G. Hansen, E. Monni, M. Hajy, S. Kartsivadze, S. Aktay, O. Tsupykov, M. Parmar, K. Deisseroth, G. Skibo, O. Lindvall, Z. Kokaia, Activity in grafted human iPS cell–derived cortical neurons integrated in stroke-injured rat brain regulates motor behavior. *Proc. Natl. Acad. Sci. U.S.A.* **117**, 9094–9100 (2020).
5. S. Falkner, S. Grade, L. Dimou, K. K. Conzelmann, T. Bonhoeffer, M. Götz, M. Hübener, Transplanted embryonic neurons integrate into adult neocortical circuits. *Nature* **539**, 248–253 (2016).
6. D. Tornero, O. Tsupykov, M. Granmo, C. Rodriguez, M. Grønning-Hansen, J. Thelin, E. Smozhanik, C. Laterza, S. Wattananit, R. Ge, J. Tatarishvili, S. Grealish, O. Brüstle, G. Skibo, M. Parmar, J. Schouenborg, O. Lindvall, Z. Kokaia, Synaptic inputs from stroke-injured brain to grafted human stem cell-derived neurons activated by sensory stimuli. *Brain* **140**, 692–706 (2017).
7. S. Grealish, A. Heuer, T. Cardoso, A. Kirkeby, M. Jönsson, J. Johansson, A. Björklund, J. Jakobsson, M. Parmar, Monosynaptic tracing using modified rabies virus reveals early

and extensive circuit integration of human embryonic stem cell-derived neurons. *Stem Cell Rep.* **4**, 975–983 (2015).
8. U. S. Sohur, P. Arlotta, J. D. Macklis, Developmental controls are re-expressed during induction of neurogenesis in the neocortex of young adult mice. *Front. Neurosci.* **6**, 12 (2012).
9. A. Mahmood, D. Lu, M. Chopp, Intravenous administration of marrow stromal cells (MSCs) increases the expression of growth factors in rat brain after traumatic brain injury. *J. Neurotrauma* **21**, 33–39 (2004).
10. Y. Zhang, M. Chopp, Y. Meng, M. Katakowski, H. Xin, A. Mahmood, Y. Xiong, Effect of exosomes derived from multipluripotent mesenchymal stromal cells on functional recovery and neurovascular plasticity in rats after traumatic brain injury. *J. Neurosurg.* **122**, 856–867 (2015).
11. L. L. Xiong, Y. Hu, P. Zhang, Z. Zhang, L. H. Li, G. D. Gao, X. F. Zhou, T. H. Wang, Neural stem cell transplantation promotes functional recovery from traumatic brain injury via brain derived neurotrophic factor-mediated neuroplasticity. *Mol. Neurobiol.* **55**, 2696–2711 (2018).
12. P. A. Walker, S. S. Bedi, S. K. Shah, F. Jimenez, H. Xue, J. A. Hamilton, P. Smith, C. P. Thomas, R. W. Mays, S. Pati, C. S. Cox Jr., Intravenous multipotent adult progenitor cell therapy after traumatic brain injury: Modulation of the resident microglia population. *J. Neuroinflammation* **9**, 228 (2012).
13. Q. Xing, A. Lin, Z. Su, C. Liu, W. Huang, W. Guo, G. Pan, Y. Guo, X. Zhong, Retrograde monosynaptic tracing through an engineered human embryonic stem cell line reveals synaptic inputs from host neurons to grafted cells. *Cell Regen.* **8**, 1–8 (2019).
14. M. T. Fitch, J. Silver, CNS injury, glial scars, and inflammation: Inhibitory extracellular matrices and regeneration failure. *Exp. Neurol.* **209**, 294–301 (2008).
15. J. Frik, J. Merl-Pham, N. Plesnila, N. Mattugini, J. Kjell, J. Kraska, R. M. Gómez, S. M. Hauck, S. Sirko, M. Götz, Cross-talk between monocyte invasion and astrocyte proliferation regulates scarring in brain injury. *EMBO Rep.* **19**, e45294 (2018).
16. J. Kjell, M. Götz, Filling the gaps—A call for comprehensive analysis of extracellular matrix of the glial scar in region- and injury-specific contexts. *Front. Cell. Neurosci.* **14**, 32 (2020).
17. A. H. Stephan, B. A. Barres, B. Stevens, The complement system: An unexpected role in synaptic pruning during development and disease. *Annu. Rev. Neurosci.* **35**, 369–389 (2012).
18. S. Hong, V. F. Beja-Glasser, B. M. Nfonoyim, A. Frouin, S. Li, S. Ramakrishnan, K. M. Merry, Q. Shi, A. Rosenthal, B. A. Barres, C. A. Lemere, D. J. Selkoe, B. Stevens, Complement and microglia mediate early synapse loss in Alzheimer mouse models. *Science* **352**, 712–716 (2016).
19. D. P. Schafer, E. K. Lehrman, A. G. Kautzman, R. Koyama, A. R. Mardinly, R. Yamasaki, R. M. Ransohoff, M. E. Greenberg, B. A. Barres, B. Stevens, Microglia sculpt postnatal neural circuits in an activity and complement-dependent manner. *Neuron* **74**, 691–705 (2012).
20. G. W. Kreutzberg, Microglia: A sensor for pathological events in the CNS. *Trends Neurosci.* **19**, 312–318 (1996).
21. M. Prinz, J. Priller, Microglia and brain macrophages in the molecular age: From origin to neuropsychiatric disease. *Nat. Rev. Neurosci.* **15**, 300–312 (2014).
22. S. Lehnard, C. Lachance, S. Patrizi, S. Lefebvre, P. L. Follett, F. E. Jensen, P. A. Rosenberg, J. J. Volpe, T. Vartanian, The toll-like receptor TLR4 is necessary for lipopolysaccharide-induced oligodendrocyte injury in the CNS. *J. Neurosci.* **22**, 2478–2486 (2002).
23. S. B. Hofer, T. D. Mrsic-Flogel, T. Bonhoeffer, M. Hübener, Experience leaves a lasting structural trace in cortical circuits. *Nature* **457**, 313–317 (2009).
24. S. Sirko, G. Behrendt, P. A. Johansson, P. Tripathi, M. Costa, S. Bek, C. Heinrich, S. Tiedt, D. Colak, M. Dichgans, I. R. Fischer, N. Plesnila, M. Staufenbiel, C. Haass, M. Snapyan, A. Saghatelyan, L.-H. Tsai, A. Fischer, K. Grobe, L. Dimou, M. Götz, Reactive glia in the injured brain acquire stem cell properties in response to sonic hedgehog. *Cell Stem Cell* **12**, 426–439 (2013).
25. S. Sirko, M. Irmler, S. Gascón, S. Bek, S. Schneider, L. Dimou, J. Obermann, D. de Souza Paiva, F. Poirier, J. Beckers, S. M. Hauck, Y. A. Barde, M. Götz, Astrocyte reactivity after brain injury: The role of galectins 1 and 3. *Glia* **63**, 2340–2361 (2015).
26. N. Mattugini, J. Merl-Pham, E. Petrozziello, L. Schindler, J. Bernhagen, S. M. Hauck, M. Götz, Influence of white matter injury on gray matter reactive gliosis upon stab wound in the adult murine cerebral cortex. *Glia* **66**, 1644–1662 (2018).
27. B. Cubelos, A. Sebastián-Serrano, S. Kim, J. M. Redondo, C. Walsh, M. Nieto, Cux-1 and Cux-2 control the development of Reelin expressing cortical interneurons. *Dev. Neurobiol.* **68**, 917–925 (2008).
28. M. Alvarez-Dolado, R. Pardal, J. M. Garcia-Verdugo, J. R. Fike, H. O. Lee, K. Pfeffer, C. Lois, S. J. Morrison, A. Alvarez-Buylla, Fusion of bone-marrow-derived cells with Purkinje neurons, cardiomyocytes and hepatocytes. *Nature* **425**, 968–973 (2003).
29. E. Brilli, E. Reitano, L. Conti, P. Conforti, R. Gulino, G. G. Consalez, E. Cesana, A. Smith, F. Rossi, E. Cattaneo, Neural stem cells engrafted in the adult brain fuse with endogenous neurons. *Stem Cells Dev.* **22**, 538–547 (2013).
30. T. Iwasato, A. Datwani, A. M. Wolf, H. Nishiyama, Y. Taguchi, S. Tonegawa, T. Knöpfel, R. S. Erzurumlu, S. Itohara, Cortex-restricted disruption of NMDAR1 impairs neuronal patterns in the barrel cortex. *Nature* **406**, 726–731 (2000).
31. T. Nakamura, M. C. Colbert, J. Robbins, Neural crest cells retain multipotential characteristics in the developing valves and label the cardiac conduction system. *Circ. Res.* **98**, 1547–1554 (2006).
32. L. Madisen, T. A. Zwingman, S. M. Sunkin, S. W. Oh, H. A. Zariwala, H. Gu, L. L. Ng, R. D. Palmiter, M. J. Hawrylycz, A. R. Jones, E. S. Lein, H. Zeng, A robust and high-throughput Cre reporting and characterization system for the whole mouse brain. *Nat. Neurosci.* **13**, 133–140 (2010).
33. I. R. Wickersham, S. Finke, K. K. Conzelmann, E. M. Callaway, Retrograde neuronal tracing with a deletion-mutant rabies virus. *Nat. Methods* **4**, 47–49 (2007).
34. J. Takatoh, A. Nelson, X. Zhou, M. M. L. Bolton, M. D. Ehlers, B. R. Arenkiel, R. Mooney, F. Wang, New modules are added to vibrissal premotor circuitry with the emergence of exploratory whisking. *Neuron* **77**, 346–360 (2013).
35. J. Thomas, M. F. Martinez-Reza, M. Thorwirth, Y. Zarb, K. K. Conzelmman, S. M. Hauck, S. Grade, M. Götz, Excessive local host-graft connectivity in aging and amyloid-loaded brain. *Sci. Adv.* **8**, eabg9287 (2022).
36. G. López-Bendito, Z. Molnár, Thalamocortical development: How are we going to get there? *Nat. Rev. Neurosci.* **4**, 276–289 (2003).
37. S. W. Oh, J. A. Harris, L. Ng, B. Winslow, N. Cain, S. Mihalas, Q. Wang, C. Lau, L. Kuan, A. M. Henry, M. T. Mortrud, B. Ouellette, T. N. Nguyen, S. A. Sorensen, C. R. Slaughterbeck, W. Wakeman, Y. Li, D. Feng, A. Ho, E. Nicholas, K. E. Hirokawa, P. Bohn, K. M. Joines, H. Peng, M. J. Hawrylycz, J. W. Phillips, J. G. Hohmann, P. Wohnoutka, C. R. Gerfen, C. Koch, A. Bernard, C. Dang, A. R. Jones, H. Zeng, A mesoscale connectome of the mouse brain. *Nature* **508**, 207–214 (2014).
38. B. Zingg, H. Hintiryan, L. Gou, M. Y. Song, M. Bay, M. S. Bienkowski, N. N. Foster, S. Yamashita, I. Bowman, A. W. Toga, H. W. Dong, Neural networks of the mouse neocortex. *Cell* **156**, 1096–1111 (2014).
39. M. Götz, S. Sirko, J. Beckers, M. Irmler, Reactive astrocytes as neural stem or progenitor cells: In vivo lineage, in vitro potential, and genome-wide expression analysis. *Glia* **63**, 1452–1468 (2015).
40. Z. Chen, W. Jalabi, K. B. Shpargel, K. T. Farabaugh, R. Dutta, X. Yin, G. J. Kidd, C. C. Bergmann, S. A. Stohlman, B. D. Trapp, Lipopolysaccharide-induced microglial activation and neuroprotection against experimental brain injury is independent of hematogenous TLR4. *J. Neurosci.* **32**, 11706–11715 (2012).
41. Á. Dénes, S. Ferenczi, K. J. Kovács, Systemic inflammatory challenges compromise survival after experimental stroke via augmenting brain inflammation, blood- brain barrier damage and brain oedema independently of infarct size. *J. Neuroinflammation* **8**, 164 (2011).
42. M. A. Erickson, W. A. Banks, Cytokine and chemokine responses in serum and brain after single and repeated injections of lipopolysaccharide: Multiplex quantification with path analysis. *Brain Behav. Immun.* **25**, 1637–1648 (2011).
43. K. Z. Chapman, R. Ge, E. Monni, J. Tatarishvili, H. Ahlenius, A. Arvidsson, C. T. Ekdahl, O. Lindvall, Z. Kokaia, Inflammation without neuronal death triggers striatal neurogenesis comparable to stroke. *Neurobiol. Dis.* **83**, 1–15 (2015).
44. L. Qin, X. Wu, M. L. Block, Y. Liu, G. R. Breese, J. S. Hong, D. J. Knapp, F. T. Crews, Systemic LPS causes chronic neuroinflammation and progressive neurodegeneration. *Glia* **55**, 453–462 (2007).
45. M. Brenner, Role of GFAP in CNS injuries. *Neurosci. Lett.* **565**, 7–13 (2014).
46. A. Elvington, C. Atkinson, H. Zhu, J. Yu, K. Takahashi, G. L. Stahl, M. S. Kindy, S. Tomlinson, The alternative complement pathway propagates inflammation and injury in murine ischemic stroke. *J. Immunol.* **189**, 4640–4647 (2012).
47. A. Alawieh, E. F. Langley, S. Weber, D. Adkins, S. Tomlinson, Identifying the role of complement in triggering neuroinflammation after traumatic brain injury. *J. Neurosci.* **38**, 2519–2532 (2018).
48. F. Roselli, E. Karasu, C. Volpe, M. Huber-Lang, Medusa's head: The complement system in traumatic brain and spinal cord injury. *J. Neurotrauma* **35**, 226–240 (2018).
49. J. Presumey, A. R. Bialas, M. C. Carroll, Complement system in neural synapse elimination in development and disease. *Adv. Immunol.* **135**, 53–79 (2017).
50. M. A. Petersen, J. K. Ryu, K. Akassoglou, Fibrinogen in neurological diseases: Mechanisms, imaging and therapeutics. *Nat. Rev. Neurosci.* **19**, 283–301 (2018).
51. M. Merlini, V. A. Rafalski, P. E. Rios Coronado, T. M. Gill, M. Ellisman, G. Muthukumar, K. S. Subramanian, J. K. Ryu, C. A. Syme, D. Davalos, W. W. Seeley, L. Mucke, R. B. Nelson, K. Akassoglou, Fibrinogen induces microglia-mediated spine elimination and cognitive impairment in an Alzheimer's disease model. *Neuron* **101**, 1099–1108.e6 (2019).
52. K. L. Pennington, T. Y. Chan, M. P. Torres, J. L. Andersen, The dynamic and stress-adaptive signaling hub of 14-3-3: Emerging mechanisms of regulation and context-dependent protein–protein interactions. *Oncogene* **37**, 5587–5604 (2018).
53. M. Foote, Y. Zhou, 14-3-3 proteins in neurological disorders. *Int. J. Biochem. Mol. Biol.* **3**, 152–164 (2012).
54. R. Hamamoto, Y. Furukawa, M. Morita, Y. Iimura, F. P. Silva, M. Li, R. Yagyu, Y. Nakamura, SMYD3 encodes a histone methyltransferase involved in the proliferation of cancer cells. *Nat. Cell Biol.* **6**, 731–740 (2004).

55. P. Kolodziej, R. A. Young, RNA polymerase II subunit RPB3 is an essential component of the mRNA transcription apparatus. *Mol. Cell. Biol.* **9**, 5387–5394 (1989).
56. S. Bonzano, I. Crisci, A. Podlesny-Drabiniok, C. Rolando, W. Krezel, M. Studer, S. de Marchis, Neuron-astroglia cell fate decision in the adult mouse hippocampal neurogenic niche is cell-intrinsically controlled by COUP-TFI in vivo. *Cell Rep.* **24**, 329–341 (2018).
57. A. Chandrasekar, F. O. Heuvel, L. Tar, A. M. Hagenston, A. Palmer, B. Linkus, A. C. Ludolph, M. Huber-Lang, T. Boeckers, H. Bading, F. Roselli, Parvalbumin interneurons shape neuronal vulnerability in blunt TBI. *Cereb. Cortex* **29**, 2701–2715 (2019).
58. K. A. Michelsen, S. Acosta-Verdugo, M. Benoit-Marand, I. Espuny-Camacho, N. Gaspard, B. Saha, A. Gaillard, P. Vanderhaeghen, Area-specific reestablishment of damaged circuits in the adult cerebral cortex by cortical neurons derived from mouse embryonic stem cells. *Neuron* **85**, 982–997 (2015).
59. J. Doerr, M. K. Schwarz, D. Wiedermann, A. Leinhaas, A. Jakobs, F. Schloen, I. Schwarz, M. Diedenhofen, N. C. Braun, P. Koch, D. A. Peterson, U. Kubitscheck, M. Hoehn, O. Brüstle, Whole-brain 3D mapping of human neural transplant innervation. *Nat. Commun.* **8**, 14162 (2017).
60. K. Kadoya, P. Lu, K. Nguyen, C. Lee-Kubli, H. Kumamaru, L. Yao, J. Knackert, G. Poplawski, J. N. Dulin, H. Strobl, Y. Takashima, J. Biane, J. Conner, S. C. Zhang, M. H. Tuszynski, Spinal cord reconstitution with homologous neural grafts enables robust corticospinal regeneration. *Nat. Med.* **22**, 479–487 (2016).
61. E. Andreoli, V. Petrenko, P. E. Constanthin, A. Contestabile, R. Bocchi, K. Egervari, C. Quairiaux, P. Salmon, J. Z. Kiss, Transplanted embryonic neurons improve functional recovery by increasing activity in injured cortical circuits. *Cereb. Cortex* **30**, 4708–4725 (2020).
62. D. Tornero, S. Wattananit, M. G. Madsen, P. Koch, J. Wood, J. Tatarishvili, Y. Mine, R. Ge, E. Monni, K. Devaraju, R. F. Hevner, O. Brüstle, O. Lindvall, Z. Kokaia, Human induced pluripotent stem cell-derived cortical neurons integrate in stroke-injured cortex and improve functional recovery. *Brain* **136**, 3561–3577 (2013).
63. K. Caeyenberghs, H. Verhelst, A. Clemente, P. H. Wilson, Mapping the functional connectome in traumatic brain injury: What can graph metrics tell us? *Neuroimage* **160**, 113–123 (2017).
64. S. A. Kirov, K. E. Sorra, K. M. Harris, Slices have more synapses than perfusion-fixed hippocampus from both young and mature rats. *J. Neurosci.* **19**, 2876–2886 (1999).
65. D. Linaro, B. Vermaercke, R. Iwata, A. Ramaswamy, B. Libé-Philippot, L. Boubakar, B. A. Davis, K. Wierda, K. Davie, S. Poovathingal, P.-A. Penttila, A. Bilheu, L. De Bruyne, D. Gall, K.-K. Conzelmann, V. Bonin, P. Vanderhaeghen, Xenotransplanted human cortical neurons reveal species-specific development and functional integration into mouse visual circuits. *Neuron* **104**, 972–986.e6 (2019).
66. Z. Petanjek, M. Judaš, G. Šimić, M. R. Rašin, H. B. M. Uylings, P. Rakic, I. Kostović, Extraordinary neoteny of synaptic spines in the human prefrontal cortex. *Proc. Natl. Acad. Sci. U.S.A.* **108**, 13281–13286 (2011).
67. B. Stevens, N. J. Allen, L. E. Vazquez, G. R. Howell, K. S. Christopherson, N. Nouri, K. D. Micheva, A. K. Mehalow, A. D. Huberman, B. Stafford, A. Sher, A. M. Litke, J. D. Lambris, S. J. Smith, S. W. M. John, B. A. Barres, The classical complement cascade mediates CNS synapse elimination. *Cell* **131**, 1164–1178 (2007).
68. A. Grosche, A. Hauser, M. F. Lepper, R. Mayo, C. Von Toerne, J. Merl-Pham, S. M. Hauck, The proteome of native adult Müller glial cells from murine retina. *Mol. Cell. Proteomics* **15**, 462–480 (2016).
69. P. Navarro, M. Trevisan-Herraz, E. Bonzon-Kulichenko, E. Núñez, P. Martínez-Acedo, D. Pérez-Hernández, I. Jorge, R. Mesa, E. Calvo, M. Carrascal, M. L. Hernáez, F. García, J. A. Bárcena, K. Ashman, J. Abian, C. Gil, J. M. Redondo, J. Vázquez, General statistical framework for quantitative proteomics by stable isotope labeling. *J. Proteome Res.* **13**, 1234–1247 (2014).
70. E. Eden, R. Navon, I. Steinfeld, D. Lipson, Z. Yakhini, *GOrilla*: A tool for discovery and visualization of enriched GO terms in ranked gene lists. *BMC Bioinformatics* **10**, 48 (2009).
71. Y. Perez-Riverol, A. Csordas, J. Bai, M. Bernal-Llinares, S. Hewapathirana, D. J. Kundu, A. Inuganti, J. Griss, G. Mayer, M. Eisenacher, E. Pérez, J. Uszkoreit, J. Pfeuffer, T. Sachsenberg, Ş. Yılmaz, S. Tiwary, J. Cox, E. Audain, M. Walzer, A. F. Jarnuczak, T. Ternent, A. Brazma, J. A. Vizcaíno, The PRIDE database and related tools and resources in 2019: Improving support for quantification data. *Nucleic Acids Res.* **47**, D442–D450 (2019).

Acknowledgments: We are grateful for the technical assistance of T. Simon-Ebert and D. Franzen. We also appreciate the expert input by J. Kjell and M. Esgleas in the proteome analysis. We are particularly thankful to M. F. Martinez-Reza for performing a crucial experiment on testing inflammatory stimuli in regard to the regulation of the G protein, which we included in the accompanying manuscript by Thomas *et al*. (*35*). **Funding:** This work was funded by the German Research Foundation to M.G. and K.-K.C. (SFB 870 "Neural Circuits") and to S.M.H. (SPP2127 HA6014-5/1), as well as Transregio 274, the EU via the NSC-Reconstruct consortium, the EraNet project Micronet, the advanced ERC grants (ChroNeuroRepair and NeuroCentro), and the Fondation Roger de Spoelberch and ERANET (Microcircuit project) to M.G., Y.Z. has received funding from the European Union's Horizon 2020 research and innovation programme under the Marie Skłodowska-Curie grant agreement No 101024862.
Author contributions: M.G. initially conceived the idea. M.G. and S.G. conceived and coordinated the project. S.G. designed, performed, and analyzed all experiments except the proteomics. J.T. and S.M.H. conducted the proteome study. J.T. performed injuries, collected samples, and post-analyzed the data. S.M.H. prepared the samples and performed measurements and quantitative analysis. For the proteome validation, glial reactivity analysis, and characterization of the identity of transplanted cells, M.T. and S.G. performed LPS and SW surgeries, and Y.Z. and S.G. performed SW followed by transplantation for the 5 dpt, 2 wpt, and 4 wpt. M.T. and S.G. stained sections, and M.T., Y.Z., and S.G. acquired images. S.G. quantified fibrinogen/C1q and GFAP/Iba1, while Y.Z. quantified Cux1 transplant composition. K.-K.C. provided expertise and viral vectors for monosynaptic tracing. S.G. and M.G. wrote the manuscript with input from all coauthors. **Competing interests:** The authors declare that they have no competing interests. **Data and materials availability:** All data needed to evaluate the conclusions in the paper are present in the paper and/or the Supplementary Materials. The MS proteomics data have been deposited to the ProteomeXchange Consortium via the PRIDE (*71*) partner repository with the dataset identifier PXD023660 and 10.6019/PXD023660.

Submitted 5 February 2021
Accepted 25 April 2022
Published 10 June 2022
10.1126/sciadv.abg9445

ScienceAdvances

Brain injury environment critically influences the connectivity of transplanted neurons

Sofia Grade, Judith Thomas, Yvette Zarb, Manja Thorwirth, Karl-Klaus Conzelmann, Stefanie M. Hauck, and Magdalena Gtz

Sci. Adv., **8** (23), eabg9445.
DOI: 10.1126/sciadv.abg9445